buildings

MDPI

Article

Thermal Modeling of a Historical Building Wall: Using Long-Term Monitoring Data to Understand the Reliability and the Robustness of Numerical Simulations

Simone Panico [1,2,*], Marco Larcher [1], Alexandra Troi [1], Cristina Baglivo [2] and Paolo Maria Congedo [2]

[1] Institute for Renewable Energies, Eurac Research, Viale Druso 1, 39100 Bolzano, Italy
[2] Department of Engineering for Innovation, University of Salento, 73100 Lecce, Italy
* Correspondence: simone.panico@eurac.edu

Abstract: Thermal modeling of building components plays a crucial role in designing energy efficiency measures, assessing living comfort, and preventing building damages. The accuracy of the modeling process strongly depends on the reliability of the physical models and the correct selection of input parameters, especially for historic buildings where uncertainties on wall composition and material properties are higher. This work evaluates the reliability of building thermal modeling and identifies the input parameters that most affect the simulation results. A monitoring system is applied to a historic building wall to measure the temperature profile. The long-term dataset is compared with the result of a simulation model. A sensitivity analysis is applied for the determination of the influential input parameters. A two-step optimization is performed to calibrate the numerical model: the first optimization step is based on an optimized selection of the database materials, while the second optimization step uses a particle swarm algorithm. The results indicate that the output of the simulation model is largely influenced by the coefficients describing the coupling with the boundary conditions and by the thermal conductivities of the materials. Very good results are obtained already after the first optimization step ($RMSE = 0.75$ °C) while the second optimization step improves further the agreement ($RMSE = 0.48$ °C). The parameter values reported in the datasheets do not match those found through optimization. Even with extensive optimization using an algorithm, starting with monitoring data is insufficient to identify material parameter values.

Keywords: thermal properties; envelope; building materials; differential sensitivity analysis; optimization

Citation: Panico, S.; Larcher, M.; Troi, A.; Baglivo, C.; Congedo, P.M. Thermal Modeling of a Historical Building Wall: Using Long-Term Monitoring Data to Understand the Reliability and the Robustness of Numerical Simulations. *Buildings* **2022**, *12*, 1258. https://doi.org/10.3390/buildings12081258

Academic Editor: Oldrich Sucharda

Received: 22 July 2022
Accepted: 15 August 2022
Published: 17 August 2022

1. Introduction

Climate change mitigation is posing significant challenges to the construction industry around the world, especially concerning the electricity generation system [1]. Building energy usage is a major concern at the European level, as it is one of the most energy-intensive sectors. Recently, the topic of smart energy communities was an example of the development of new models that would innovate and reconfigure the energy system [2]. According to [3], buildings consume 40% of primary energy and produce 36% of greenhouse gas emissions, with some member states exceeding 45%. This is why it is essential to promote greater energy efficiency, which also has the advantage of improving thermal comfort for users [4]. Numerical modeling of buildings or building components is a widely used approach to design and propose targeted energy-efficient solutions. One of the crucial questions is how well the results of numerical simulations match reality. Furthermore, it is generally difficult to determine the simulation inputs with certainty [5]. Indeed, neglecting the uncertainties and variabilities of several parameters can affect the reliability and robustness of the results and lead to wrong final design decisions [6]. The more accurate the input data, the more reliable results the simulation returns [7,8].

Numerical simulation of historical buildings makes it possible to target effective interventions to make them more energy efficient, also considering impending climate change. [9]. Hence, simulations are often carried out at the level of the wall component. The correct modeling of a dynamic simulation of historical buildings is therefore crucial. For the envelope, it is necessary to know how the stratigraphy is composed, in particular the type of materials, their properties, and their thickness within the structure. Typically, if the material is not included in the materials' database, material properties for the numerical model are chosen from technical standards or a commercial data-sheet, leading to significant uncertainties in the evaluation [10]. In the case of ancient components, this operation is even more complex. Indeed, building materials are vulnerable to deterioration and decay over time [11] and this makes their characteristics unique. It therefore becomes a challenge to find a correspondence between the real ancient material and those listed in standards and/or in software databases [12,13].

In the reviewed studies, the input parameters of the materials and coefficient values of the boundary conditions were often investigated with laboratory tests on samples and subsequently considered known. Another approach would be to apply an inverse methodology that tries to calibrate the numerical model starting from the monitored data [7]. Ibrahim et al. [14] state that using numerical models relating to data measured in the laboratory is not sufficient and can lead to large deviations from actual in-situ conditions, so calibration is necessary to enable numerical models to reproduce reliable results.

In the literature, many studies have tested the reliability of numerical simulations by making comparisons with monitored data [14–21].

Other studies use the monitored data to perform a calibration to obtain a more reliable predictive tool. Calibration is often carried out by changing some input parameters. Some studies apply the calibration to a zone model [17,22]. Sadłowska-Sałęga et al. [23] state that simulation without model calibration can give unacceptable results and therefore calibration is essential to achieve accurate calculations.

Some studies have instead performed a calibration at the component level using sensors embedded in the stratigraphy [7,24]. A calibration using material parameters was carried out by Panico et al. [25] in which different material parameters were varied serially to optimize the model in Delphin to obtain results more similar to those monitored. Since numerical models can have many input parameters, often only the most influential ones are varied in the calibration process. For this reason, a sensitivity analysis (SA) is often carried out [26–29]. In some cases, the sensitivity analysis is used in the post-calibration phase [30,31]. Instead, model calibration is often carried out using optimization algorithms applied to a parameter found to be influential through sensitivity analysis. Calibration makes it possible to reduce the discrepancy between simulation results and monitored data [7,10,26,28,31–34].

Among the articles reviewed, very few works were found that aim to calibrate and apply SA to a thermal simulation model and, above all, a comparison with long-term monitored data was missing. At the component level, no work has been found in the literature that approached a differential sensitivity analysis (DSA) or a calibration (using an optimization algorithm) to compare the results of a simulation with real values of sensors placed in different layers in the stratigraphy of a historical wall.

The novelty of this study regards the application of a methodology for calibration of a dynamic thermal simulation model applied to the component wall of historic stone-masonry (which underwent an energy retrofit intervention) supported by long-term monitoring.

The aim of the paper is twofold: firstly, the sensitivity analysis quantifies the input parameters that affect the result of the simulation the most, indicating the parameters that should be more accurately determined when setting up the numerical model. Secondly, the optimization process is used to select the "optimal" values of these input parameters and to quantify the reliability that the numerical model can reach in reproducing the monitored

data. Furthermore, an effort is made to determine whether using an optimization technique in combination with simulation software could be the recommended method for calibrating the numerical model with respect to input parameters and if the obtained results can lead to values that are comparable with the known ones.

2. Methodology

The methodology is summarized in the flowchart shown in Figure 1.

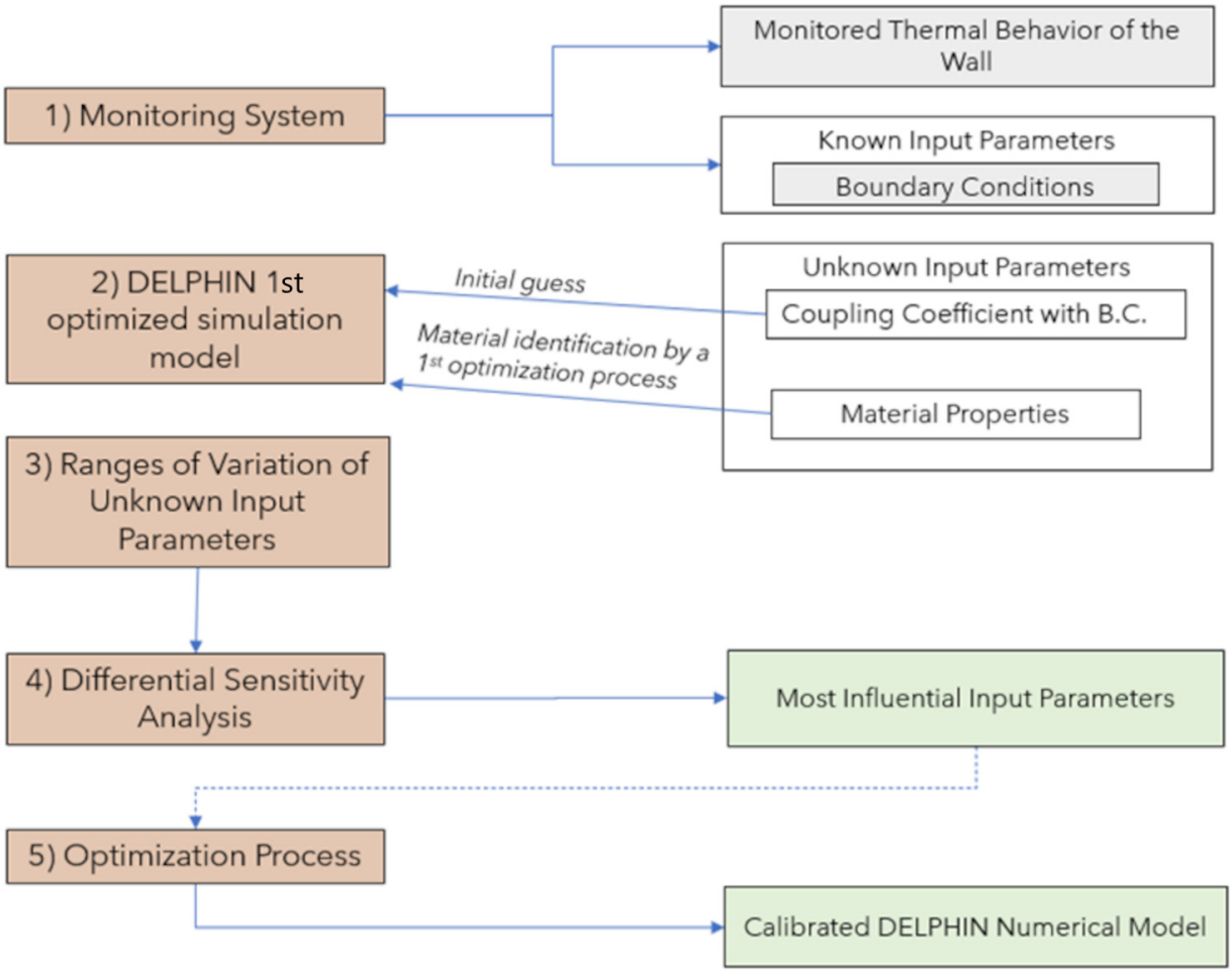

Figure 1. Flowchart of the methodology.

The single steps are explained below:

1. The first step consists of setting up the monitoring system that provides a long-term analysis of the thermal behavior of the historic wall under analysis.
2. The software Delphin 6.1 [35] is used to set up the numerical model of the wall (at the component level). Since several input parameters of the simulation are unknown at this stage, several simulations were carried out by varying the materials in the database and choosing those that reduced the difference between the simulation values and those obtained from the monitoring system. The simulation with the optimal materials identified in this way was identified as the first optimized simulation.
3. The definition of the variation range with each unknown input parameter of the numerical model. This process is done using different sources such as scientific literature, datasheets and software databases, national and international standards, and laboratory measurements. The outcome of this step is a variation range for each unknown input parameter.

4. Use of sensitivity analyses (SA) to identify which of the input parameters are the most influential (or are negligible) for the calibration of the numerical model. In particular, the differential sensitivity analysis (DSA) is applied.
5. Model calibration using the optimization program GenOpt. The optimization algorithm is set to reduce the discrepancy between simulated and monitored data. The final output of the optimization process is the calibrated model and the definition of all the unknown input parameters.

2.1. The Case Study

The case study is a historical residential building (Figure 2) located in Settequerce/Siebeneich (BZ), North Italy.

Figure 2. Plan overview of the analyzed building. The location of the wall that was examined for this study is indicated by the arrow.

According to the Italian climate classification, the location falls in the climatic zone E, characterized by 2771 heating degrees day (this value is referred to the closest city of Terlano). For the international classification proposed by Köppen [36], it falls in the climate class Dfb defined as a warm summer humid continental climate.

This work is focused on the thermal behavior of one of the walls of the building which is exposed to North–East with an azimuth of 62° from the North (as marked by the arrow shown in Figure 2). The area bounded by the monitored wall is used as a warehouse and storage room.

Figure 3 shows the stratigraphy of the monitored wall, which is composed of existing (historical) materials and new materials installed during a recent retrofit intervention (2017). Before the renovation, the existing wall configuration consisted of 4 cm thick external plaster, 44 cm of red porphyry masonry, and 1.5 cm internal plaster.

The addition of the other layers occurred during the energy retrofit of the building. An 8 cm thick wood fiber panel was added on the internal side and was adhered to the old plaster using a clay-based adhesive mortar about 1 cm thick. In addition, the renovation phase included the application of lime-based plaster both on the internal (1.5 cm) and external (2 cm) facades.

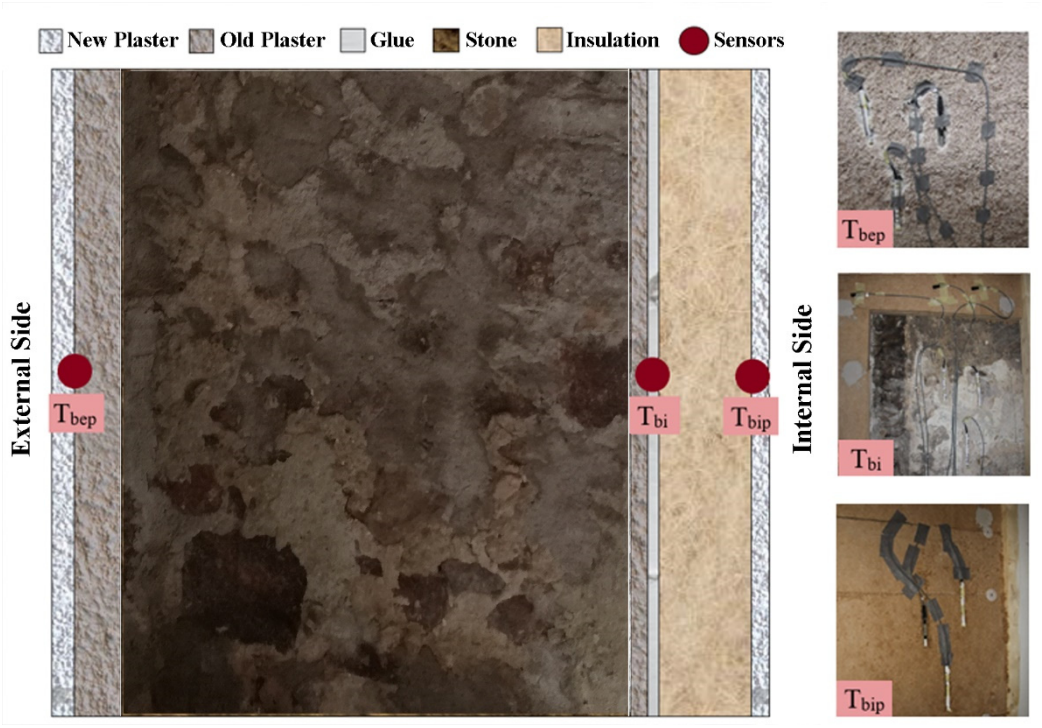

Figure 3. Monitored wall and internal sensors installed.

2.2. Monitoring System

The monitoring system is designed to monitor the external climate of the location, the interior climate of the building, and the thermal conditions within the wall. A picture of the analyzed facade is shown in Figure 4a.

Figure 4. (**a**) Northeast wall monitored. (**b**) External sensors installed (Pyranometer, T/RH sensor, Surface temperature sensor).

The external climate is monitored using temperature (T) and relative humidity (RH) sensors (E + E EE060), surface temperature sensors (thermocouples), and a pyranometer (Hukseflux SR05) for the acquisition of incident solar radiation, installed on the wall as shown in Figure 4b.

A stand-alone temperature and relative humidity sensor (E + E HUMLOG 20) is placed in the inner room and provides all the required information on the interior climate.

Figure 5a shows in orange the daily averaged internal temperatures measured by the stand-alone sensor positioned in the room adjacent to the monitored wall. Figure 5b shows the temperature data recorded for the entire monitored period by the sensor installed on the external wall (the photo of the sensor is shown in Figure 4b). In the two graphs, hourly averaged values were also plotted using the dashed lines. These graphs provide an overview of the thermal influences to which the component is subjected. During the cold months, the internal temperature is almost constant at a value of less than 22 °C, while during the summer months there are considerable fluctuations and temperatures with peaks of more than 28 °C. This is because the room is used as a storage room and is thus rarely used by tenants.

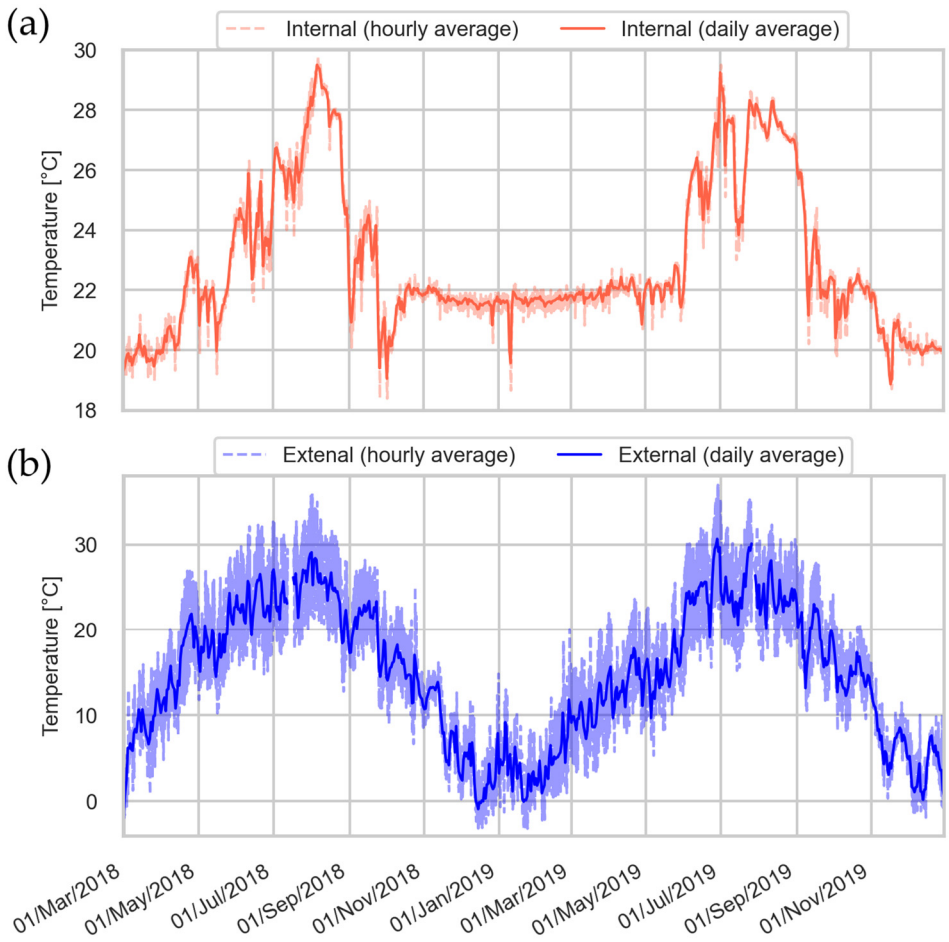

Figure 5. Development of hourly and daily temperatures measured on the inside (**a**) and outside (**b**) of the wall under analysis over a period of 22 months.

Combined temperature and relative humidity sensors placed at the interfaces between the different materials are installed to monitor the thermal conditions within the wall. Figure 3 shows the exact position of the sensors:

- T_{bep} denotes the position of the sensors located on the outermost side of the stratigraphy, between the pre-existing old plaster and the new plaster.
- T_{bi} indicates the position of the sensors placed in the layer of glue used for the installation of the insulation.
- T_{bip} specifies the position of the sensors closest to the inside of the house. These have been fixed above the insulation and are located under the plaster layer applied to the interior surfaces.

Three sensors were placed in each of the positions mentioned above. This had a double purpose: having more sensors is a precautionary measure in case of breakage, and it also allows to collect more information about the possible effect due to the inhomogeneity of the stratigraphy (and in particular of the historical wall). One of the three sensors broke at each of the monitored locations, leaving two working sensors per layer.

The installation of these sensors took place during the renovation phase; therefore, it was possible not to drill holes in the wall, avoiding the formation of thermal bridges that could affect the reliability of the measured data. All sensors communicate via cable with a control unit for data acquisition and recording. The data used for this work covers 1 year and 9 months (from 25 March 2018 to 29 December 2019). Although the monitoring system provides complete hygrothermal monitoring of the wall, here the focus will be only on the thermal analysis, to reduce the complexity of the problem. Furthermore, a reliable output of the temperature behind the insulation ensures a good assessment of interstitial condensation. The evaluation of the coupled thermal and hygrometric behavior will be addressed in future works.

2.3. Thermal Wall Modeling in Delphin

The simulation software Delphin 6.1 is used to model the wall. The input parameters required to run the simulation are reported in Table 1. Some of the input parameters, and in particular the boundary conditions (external and internal climatic conditions), are measured directly by the monitoring system and therefore they are considered known. The other parameters, i.e., the material properties and the coefficients that describe the coupling of the wall with the boundary conditions are not known exactly, therefore there is an associated uncertainty, and they are considered unknown input parameters.

Table 1. Sources of the input values in the simulation.

Input Parameters		Known/Unknown	Sources ("First Optimized Simulation")
External climatic conditions	Temperature	Known	Monitoring System
	Short Wave Solar Radiation	Known	Monitoring System
Indoor climatic conditions	Temperature	Known	Monitoring System
Wall Model	Thermal Conductivity (5 materials)	Unknown	Delphin Database + Preliminary Optimization
	Specific Heat Capacity (5 materials)	Unknown	Delphin Database + Preliminary Optimization
	Density (5 materials)	Unknown	Delphin Database + Preliminary Optimization
Boundary coefficients	Convective heat transfer coefficient (Internal)	Unknown	WTA Recommendations 6.2 [37]
	Convective heat transfer coefficient (External)	Unknown	WTA Recommendations 6.2 [37]
	The solar absorption coefficient for short wave radiation	Unknown	DIN 18599 [38]

The initial conditions of the simulation model are not considered a relevant input parameter. This is because it was decided to start the comparison period between simulated and monitored data with a delay of 2 months with respect to the actual start of the monitoring system and of the simulation. Therefore, the choice of the initial conditions of the simulation has a negligible impact on the thermal behavior of the wall within the comparison period.

The output provided by the Delphin simulation model is the temperature profile within stratigraphy as a function of time. In particular, the temperature can be calculated also at the same position where the monitoring sensors are installed giving the possibility

to compare numerical and experimental data. The statistical index used to assess the agreement between monitored and simulated data is described in the following section.

2.3.1. Statistical Index

A widely used statistical index to compare experimental measures and dynamical numerical simulations is the root mean square error (RMSE) [39]. To include the measurement uncertainty, a normalized RMSE, χ_{RMSE}, is defined as follows:

$$\chi_{RMSE} = \sqrt{\frac{1}{N}\sum_{i}^{n}\left(\frac{T_{i,mon} - T_{i,sim}}{e_{T_{i,mon}}}\right)^2}, \quad (1)$$

where:

- $T_{i,mon}$ is the temperature recorded by the sensors;
- $T_{i,sim}$ is the hourly outcome in terms of temperature from the simulation;
- $e_{T_{i,mon}}$ is the measurement uncertainty calculated as the maximum value between the instrument accuracy (± 0.3 °C) and the standard deviation (σ) between sensors placed in the same layer.

The χ_{RMSE} index is calculated for each position in the stratigraphy. The statistical indices referring to the position of T_{bep}, T_{bi}, T_{bip} are $\chi_{T,bep}$, $\chi_{T,bi}$, *and* $\chi_{T,bip}$, respectively. The χ_{avg} value represents the average of the three calculated indices. A value of the χ_{RMSE} index smaller than one indicates a generally good agreement between simulated and monitored data since the average deviation between the two datasets is of the order of the experimental uncertainty.

2.3.2. Materials and Parameters Selection for the First Optimized Simulation

A reverse approach was used, with data from the monitoring system being used to identify the materials. The initial set of materials was searched in order to obtain a reliable simulation in terms of the difference between the output and the monitored values. The authors assumed that the materials' information level was limited to material typology in this study (plaster, stone, etc.).

Each material type assigned to the numerical model was varied within the corresponding category. The material variations were as follows: stone-new plaster-old plaster-glue. The only material that was not varied was the insulation because the authors had sufficient information on the installed material. The authors recognize that using a serialized optimization does not provide the best possible combination. At the same time, it achieved the goal of obtaining a first optimized simulation with output values that were sufficiently close to those monitored. Section 3.2 contains the values of the parameters used for the materials as well as the coefficients of the boundary conditions.

2.4. Differential Sensitivity Analysis (DSA)

The SA represents the study of how uncertainty in the output of a numerical model can be attributed to different sources of uncertainty in the model input [40].

The differential sensitivity analysis (DSA) is used to investigate the influence of each parameter by considering the deviations between simulated and monitored data in each of the three monitoring positions within the stratigraphy. Starting from the first optimized simulation, the input parameters are varied one at a time. The varied parameters are those marked as "Unknown" in Table 1, and the variation ranges are specified in the next two subsections.

2.4.1. Range Selection of Materials Parameters

In numerical analyses, the choice of material properties can be made using datasheets, but this choice may involve uncertainties such as:

- Uncertainty in the measurement result (typically not expressed in the datasheet);

- Uncertainty in the source used to provide the number in the datasheet (often datasheet reports a number without a reference standard or methodology and in some cases, the number might not even correspond to a measured value);
- Uncertainty in the installation procedure which might influence the material property;
- Uncertainty associated with the effect of ageing, moisture, and temperature.

There are no technical specifications for historical materials. In this case, samples can be collected on-site and measured in the laboratory. This procedure is both expensive and time-consuming, and it is not always feasible. Furthermore, measurements of some samples may not be representative due to the significant heterogeneity of historic materials. This increases the uncertainty associated with material properties.

Hence the decision for a wide choice of sources for the definition of the ranges of variation for each input parameter was conducted through:

- Commercial technical datasheets (if available);
- International standards;
- Databases of hygrothermal simulation software;
- Scientific literature;
- Laboratory measurements.

A total of 18 parameters are taken into account: 3 thermal properties for each of the 5 materials that comprise the wall and 3 related to the wall's coupling with the boundary conditions (convective heat transfer coefficient and solar radiation absorption coefficient).

The selection of variation ranges for each parameter is critical for producing an accurate SA. They must be representative and accurate. The selection of variation ranges for each parameter was thoroughly researched.

Some considerations are made for the selection of the considered range for each parameter (references used for range selection are indicated in Tables 2 and 3). For instance, regarding the thermal conductivity value (λ) of the insulating layer (consisting of a wood fiber panel), the upper value of the range is determined by increasing the value reported in the technical datasheet (0.043 W/mK) to include measurements uncertainties and uncertainties related with the installation process. Referring to the study of H.-J. Choi et al. [41], in which a percentage increase in λ-value of 42.7% is reported, the upper limit is set to 0.061 W/mK. The lower limit is set to 0.038 W/mK, which is the smallest value reported in UNI 10351 [42] for wood fiber insulation.

Table 2. Range of variation of material parameters.

Materials		New Plaster	Old Plaster	Glue	Stonemasonry	Insulation
C_p (J/kgK)	Initial	999.2	1417.7	889	708	2000
	min/max	630/1500 [35]	630/1500 [35]	772.2/1461.2 [35]	531/1348 [35], (Lab measures)	1000/2100 [42], (Datasheet)
	Step-size	30	30	23.8	28.2	37.9
ρ (kg/m^3)	Initial	1200	1520	1673	1919	150
	min/max	1035/1600 (Datasheet), [35],[46]	600/1800 [46]	561/1753 [35]	1494/2443 [45],[35] (Lab measures)	40/250 [46]
	Step-size	19.5	41.3	41.1	32.7	7.2
λ (W/mK)	Initial	0.28	0.62	0.72	2.00	0.042
	min/max	0.18/0.80 [46]	0.28/0.82 [35],[29]	0.12/1.10 [35], (Datasheet)	1.13/2.62 [45],[44],[43], (Lab measures)	0.038/0.061 [41],[42]
	Step-size	0.02	0.02	0.03	0.05	0.001

Table 3. Range of variation of boundary coefficients.

Boundary Coefficients	Initial	h_{int} (W/m^{2}K) 8	h_{ext} (W/m^{2}K) 17	α_{sol} (-) 0.4
	min/max	4/10.6 [37],[47]	11.9/17 [37],[47]	0.2/0.6 [35],[48]
	Step-size	0.34	0.26	0.02

Because it is made up of a combination of stones and mortar, simulating the stone masonry layer is a complicated task. The authors decided to refer to the work [43] and consider wider ranges of variation in the mortar/stone ratio. In general, spreading the properties of the stone to those of the entire stone-masonry can lead to significant biases, even though it allows a substantial reduction in simulation time [44]. For this reason, a homogenized porous medium approach [45] was preferred, which was shown to be as fast as a one-dimensional simulation but at the same time lead to accurate results. In this study, the approach followed for the definition of the ranges of variation of the thermal parameters of the stone masonry layer considers the combined presence of stone and mortar. The values of the stone alone are tested in the laboratory, obtaining the following results which include the uncertainty of the tests:

- Specific heat (C_p) equal to 700 J/kgK (with the error of ±20%);
- Density (ρ) equal to 2450 kg/m^3 (with the error of ±100 kg/m^3);
- Thermal conductivity (λ) equal to 2.65 W/mK (with the error of ±10%).

The material properties of the mortar are taken from the Delphin database. Considering first the minimum and then the maximum values achieved for the two materials, a weighted average is performed. This procedure is followed for C_p, ρ, and λ, although with some differences exposed below:

- For density, a weighted average based on volume percentages is used
- For specific heat capacity, a weighted average based on mass percentages is used [45]
- For thermal conductivity, the weighted average is not the correct approach and in general an accurate derivation would require dedicated simulations [45]. However, in this context, there are already several other uncertainties and since the methodology is applied for the definition of variation ranges, a volume-weighted average approach is considered suitable. Based on the results obtained in [45], it has been assessed that this simplified methodology can lead to an overestimation of the thermal conductivity of the homogenized porous medium by approximately 22%. This effect is taken into account by decreasing the lower limit of the variation range by 22%.

2.4.2. Range Selection of Boundary Coefficients

The choice of the range of variation of the internal convective heat transfer coefficient (h_{int}) is based on UNI EN ISO 13788 and WTA Recommendations 6.2. The minimum value of the range is fixed at 4 W/m^{2}K while the maximum value is set at 10.5 W/m^{2}K. For the external convective heat transfer coefficient (h_{ext}), the lower limit of the range is set to 11.6 W/m^{2}K, and the upper value chosen is 17.0 W/m^{2}K, following WTA 6.2 recommendations. The range of variation of the absorption coefficient for short waves radiation (α_{sol}) ranges from 0.2 (which corresponds to a bright surface) to 0.6 (which corresponds to muted pair surface). Table 2 shows the variation ranges, variation steps, and initial values used in the DSA for the material properties (C_p, ρ, λ) of each material composing the analyzed wall. Table 3 shows the same parameters for the coefficients describing the coupling with the boundary conditions: internal (h_{int})/external (h_{ext}) heat coefficient and solar absorption coefficient (α_{sol}).

2.5. Thermal Optimization

The sensitivity analysis supported the identification of the parameters that affect the most the output of the simulation model. Then, an optimization process is performed to find the values of these parameters which minimize the index χ_{RMSE}. All parameters are varied through the GenOpt software [49] using the GPSPSOCCHJ algorithm, a hybrid optimization algorithm composed of PSO (particle swarm optimization) and GSP (Hooke-Jeeves generalized pattern search). A script in Python is implemented to vary all the parameters present in Delphin, run the simulation, and calculate the χ_{RMSE} index. The script is then read by GenOpt generating a model with parameter values varying in a defined range [10].

To reduce the computational time, the number of parameters to be varied is reduced by using only those that are found to be most influential in the DSA. The range of variation of each parameter corresponds to that used for the DSA.

Because the model of heat transport in Delphin does not depend on the density and on the specific heat capacity individually but only on their product, i.e., the volumetric heat capacity (c_{vol}), a further simplification is made. In the optimization process, only the volumetric heat capacity is varied as an input parameter (and not the specific heat capacity or the density individually), reducing in this way the number of parameters to be varied.

3. Results and Discussion

This section first discusses the results of the sensitivity analysis, which are subsequently used to define the input parameters of the optimization. Thereafter, it provides the results of the second optimization process.

3.1. Sensitivity Analysis

The results of the DSA are shown using a box plot. Figure 6 presents the values of χ_{RMSE} for each sensor placed in the stratigraphy $\chi_{T,bip}$, $\chi_{T,bi}$, $\chi_{T,bep}$. Figure 7 shows the value of χ_{avg} obtained from the average of the three indices. For each sensor, the χ_{RMSE} index describes how close the simulation output values are to the monitored values; a smaller χ_{RMSE} value indicates a closer match. The red dashed line indicates the value of the χ_{RMSE} index obtained with the first optimized simulation. Each parameter is represented by a different color in the box plot. The width of each box indicates how the output varies as the parameter changes within the predefined range. A greater width indicates that the parameter has a greater influence on the considered index shown on the y-axis. A box plot displays the five values that summaries the χ_{RMSE} obtained. The minimum, first quartile, median, third quartile, and maximum are shown in the box plot.

Regarding the sensor $\chi_{T,bip}$ in Figure 6, it is possible to notice that the most influential parameters are the coefficient h_{int} and the thermal conductivities (λ) of the insulation layer and the new plaster. It is noticeable that varying the parameters of the old plaster, glue, and stone (except slightly for λ_{stone}) does not affect the value of $\chi_{T,bip}$ significantly. Moreover, it can be observed that by changing individually the values of $\lambda_{Insulation}$, $\lambda_{New\ Plaster}$ and h_{int} it is possible to obtain a reduction of the index $\chi_{T,bip}$ for the first optimized simulation.

For $\chi_{T,bi}$ in Figure 6, the thermal conductivity (λ) of all the materials plays a key role in the thermal analysis. Stone masonry has the most important influence on stratigraphy being the element that provides the thermal mass. In fact, its density (ρ) and specific heat capacity (C_p) are also significant parameters. Moreover, in this position underneath the insulation, it is crucial the choice of the correct value of the external convective heat transfer coefficient (h_{ext}) and the value of the solar radiation absorption coefficient (α_{sol}). This is unexpected because the sensors are positioned at a depth of about 50 cm from the external surface, indicating that the point behind the insulation is more dependent on the outside than on the inside. This could be because the insulation has a "screening" effect on the inside. In other words, the temperature behind the insulation is highly correlated with external temperature but only weakly correlated with internal temperature (due to

the effect of the insulation), which may result in the sensitivity analysis emphasizing the influence of external parameters.

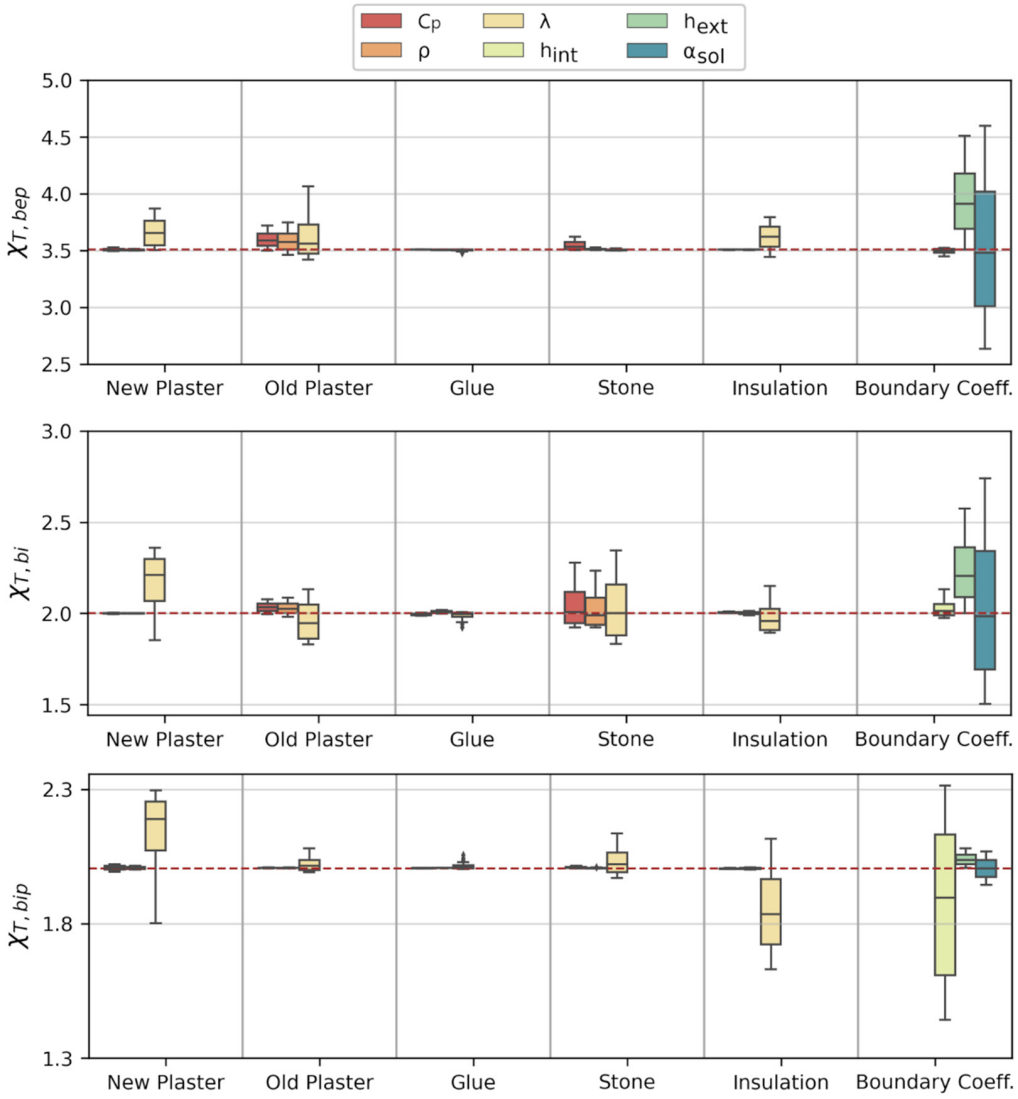

Figure 6. DSA for each monitored position (T_{bep}—temperature behind the external plaster, T_{bi}—temperature behind the insulation, T_{bip}—behind the internal plaster) in the stratigraphy.

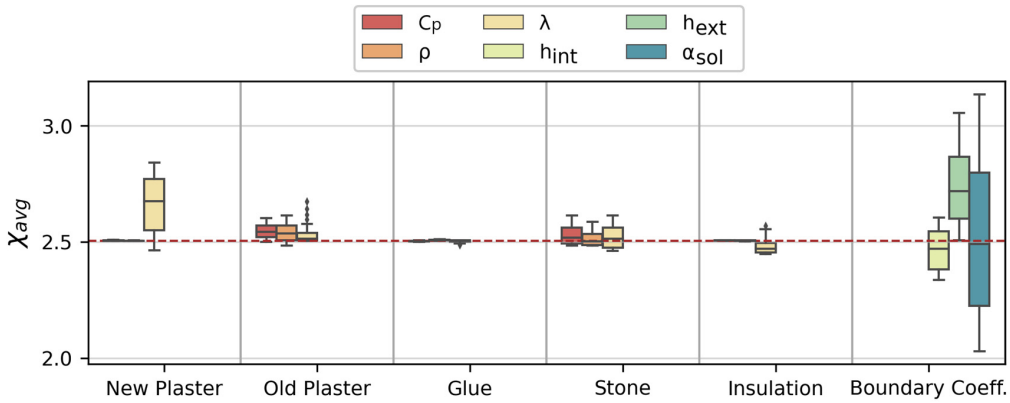

Figure 7. DSA for the average value of the three positions in the stratigraphy.

Regarding $\chi_{T,bep}$ in Figure 6, as expected, the choice of the coupling coefficients of the wall with the external climate, h_{ext}, and α_{sol}, strongly influences the simulation output. The thermal conductivity is the material parameter that most influences the results also, in this case, especially the one of the insulation, the new plaster and the old plaster. In this case, the thermal parameters of the stone are the least influential (together with the glue). The conductivity of the insulation is again an important parameter. This indicates that it is relevant to the thermal flow from inside to outside (and vice versa). As the sensor is positioned between the two external plasters, their parameters, as expected, play a significant role.

There are parameter combinations that lower the overall χ_{RMSE} value showing that there is a potential for improvement with respect to the first optimization process. Looking at the averaged value it is evident that the choice of α_{sol} can consistently change the result. As it is evident from Figure 7 (χ_{avg}), the glue parameters do not affect the thermal simulation results as well as the density and specific heat of the new plaster and insulation. These parameters will not be varied during the second optimization phase.

3.2. Results of the second Optimization

By using the software GenOpt with the genetic algorithm, a total of 3920 simulations were performed during the second optimization process. Some parameters were not taken into account during the optimization process because they were found to have a negligible influence on the numerical model using the sensitivity analysis. Material parameters and boundary condition coefficients were optimized in order to reduce the value of χ_{RMSE}. Through optimization (second optimization process), it was possible to determine the material parameter and boundary coefficient values that reduced the differences between the output of the numerical model and the monitored data. Table 4 shows the comparison of material properties obtained from the first optimized simulation and the second optimization process. In addition, the table reports the variation range and, when available, the values from the datasheet or laboratory measurements. For the new plaster and the insulation, the parameter C_{vol} has not been varied since was found to have little influence from DSA. Table 5 shows the same values for the boundary coefficients.

Table 4. Overview of the result of the second optimization step: range of variation, best solution, and datasheet or laboratory values, in terms of thermal conductivity (λ) and volumetric heat capacity c_{vol}. The *symbol* "-" is used when no values are provided or no tests were carried out.

Materials	λ [W/mK]				c_{vol} [kJ/m^{3}K]			
	First Optimized Simulation (Initial Value)	Range (min-max)	Second Optimized Value	Datasheet/Lab Value	First Optimized Simulation (Initial Value)	Range (min-max)	Second Optimized Value	Datasheet/Lab Value
New Plaster	0.28	0.18 0.80	0.32	<0.63/-	1199	- -	-	-
Old Plaster	0.62	0.28 0.82	0.79	-/-	2155	378 2700	2631	-/-
Stone masonry	2.00	1.13 2.60	1.18	-/2.65 (only stone)	1359	793 3293	1272	-/1691 (only stone)
Insulation	0.042	0.038 0.061	0.040	0.043/-	300	- -	-	-

A comprehensive evaluation of the optimization process together with the index χ_{RMSE}, also the root mean square error, $RMSE$, and the mean absolute error, MAE, are calculated. Their values are shown in Table 6 for each monitored position, both for the first optimized simulation model and for the second optimized simulation model.

Table 5. Overview of the first optimized simulation, range of variation, best solution, guidelines, or standard value for the boundary coefficients.

Materials	Boundary Coefficients			
	First Optimized Simulation	Range (min-max)	Second Optimized Value	Guidelines [37]
h_{int} [W/m^{2}K]	8	4 10.6	4.14	8
h_{ext} [W/m^{2}K]	17.0	11.9 17	17	17
α_{sol} [-]	0.4	0.2 0.6	0.205	0.4

Table 6. Statistical index RMSE, MAE and χ_{RMSE} for each position. First optimized simulation (left column) and second optimized simulation are compared with the value given from [39] for a LV1 accuracy.

Statistical index	Position	First Optimized Simulation		Second Optimized Simulation		Limit for lv1 Quality According [39]
		Index Value	Average Value	Index Value	Average Value	
$RMSE$ [°C]	T_{bip}	0.60	0.75	0.39	0.48	<1
	T_{bi}	0.60		0.34		
	T_{bep}	1.06		0.70		
MAE [°C]	T_{bip}	0.54	0.65	0.33	0.38	<1
	T_{bi}	0.48		0.23		
	T_{bep}	0.92		0.57		
χ [-]	T_{bip}	2.01	2.51	1.30	1.59	
	T_{bi}	2.00		1.14		
	T_{bep}	3.51		2.33		

The evaluation of the index χ_{RMSE} can be done having in mind that a value of χ_{RMSE} close to 1 indicates that the discrepancy between the simulated and monitored curves is of the same order of magnitude of the measurement uncertainty, indicating an almost perfect agreement. The MAE and $RMSE$ values, are instead evaluated using the two different levels of accuracy proposed by Huerto-Cardenas et al. [39], where the threshold for each index is: Level 1 (<1 °C) corresponding to "high accuracy" and Level 2 (<2 °C) to "low accuracy".

Table 6 shows that the results obtained with the first optimization step are already very good displaying a χ_{avg} equal to 2.51 and an average value of $RMSE$ and MAE of 0.75 °C and 0.65 °C, respectively, which correspond in both cases to a high accuracy level, according to the categorization proposed by Huerto-Cardenas et al. [39]. The second optimization step reduces further the values of these three indexes ($\chi_{avg} = 1.59$, $RMSE = 0.48$ °C, $MAE = 0.38$ °C) indicating a final excellent agreement.

Considering the individual positions, it can be observed that the best agreement is obtained in the layer between the insulation and the existing wall, T_{bi}. This is good considering that having a robust determination of the temperature behind the insulation in hygrothermal simulations is beneficial for the evaluation of the formation of interstitial condensation. On the other hand, regarding the external position in the stratigraphy, T_{bep}, even if the obtained agreement is still good, it can be observed that is the most difficult curve to calibrate. This is justified by the fact that this position is significantly affected by the coupling with strongly changing boundary conditions, i.e., exterior temperature and sun radiation.

These considerations are confirmed also by looking at the detail of the variation of the temperature values in the three positions. The top panel of Figures 8–10 shows the monitored temperature curves (red with the shadowed air of the uncertainty), the

simulated curves after the first optimization step (green), and those obtained after the second optimization step (blue). The bottom panel of Figures 8–10 shows the hourly difference between the monitored values and those derived from the two simulations:

$$\Delta T_i = T_{mon,i} - T_{sim,i}, \quad (2)$$

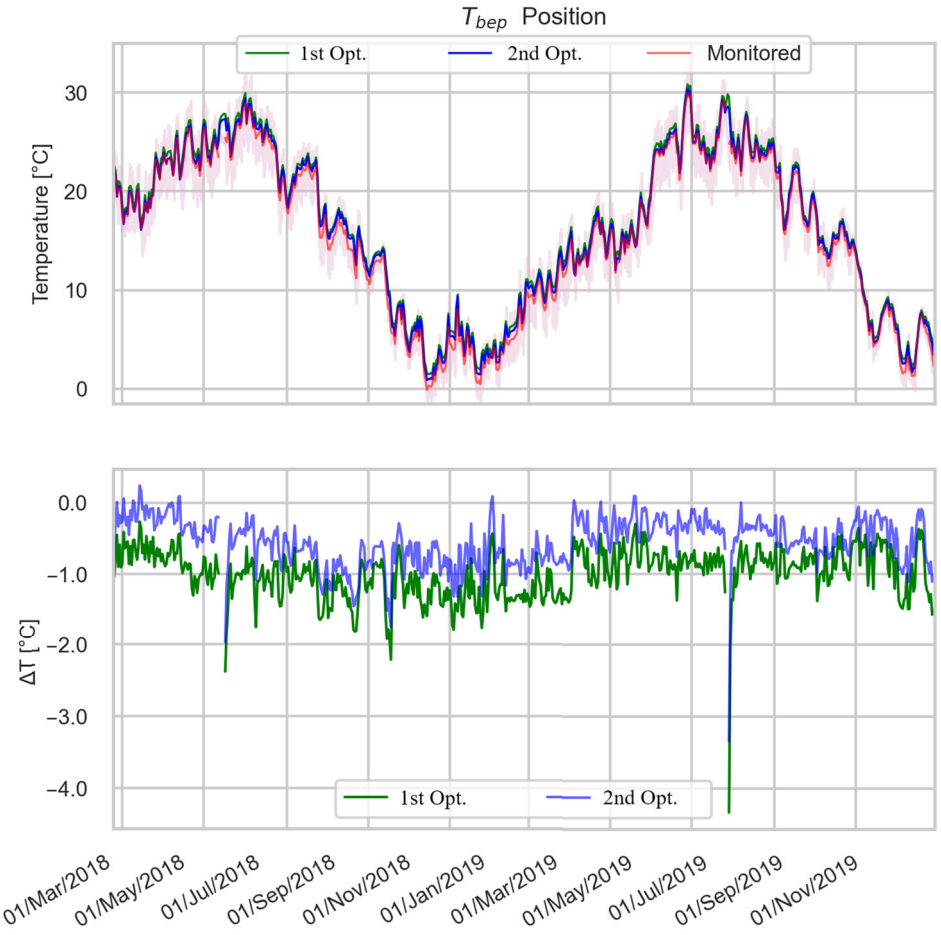

Figure 8. Comparison of the curve of the monitored temperature values at position T_{bep} (in red including the shadow air of the measurement uncertainty) with the curve of the first optimized simulation (in green) and the second optimized simulation (blue).

In this equation, i indicates the i-th hour considered during the entire period, T_{mon} the monitored temperature, and T_{sim} the temperature obtained with the simulation. The closer the values of ΔT_i are to zero, the greater the agreement between monitored and simulated data. Positive values indicate that the monitored temperature is higher than the simulated temperature and vice versa. The peaks present in June 2018 and September 2019 in the graphs are due to the lack of monitored data.

Figure 8 shows the behavior of the temperature values referring to position T_{bep}, i.e., the one referring to the sensor placed on the exterior side. Because the sensor is installed 2 cm beneath the external plaster, it is subjected to greater thermal variation, as shown by the high fluctuation of the curve in Figure 8. The first optimized simulation curves have a larger error throughout the monitored period. The second optimized simulation greatly reduces the difference when the ΔT_i is negative (simulated temperatures higher than monitored), especially in the winter months. The simulated temperature curves typically show higher values than the monitored ones. This effect is reduced in the second optimized

simulation due to the reduction of the α_{sol} value. In general, the shift of the simulated curve towards the monitored one with the second optimization step is evident.

Figure 9 relates to the sensor in position T_{bi}. Since the temperature behind the insulation is mainly driven by the coupling with the external environment, the first optimization simulation reports temperature values that are almost always higher than those monitored. As seen above, the difference between the monitored data is mostly less than 1 °C. Nevertheless, the second optimization process further improves the agreement, bringing the simulated temperatures closer to the monitored ones.

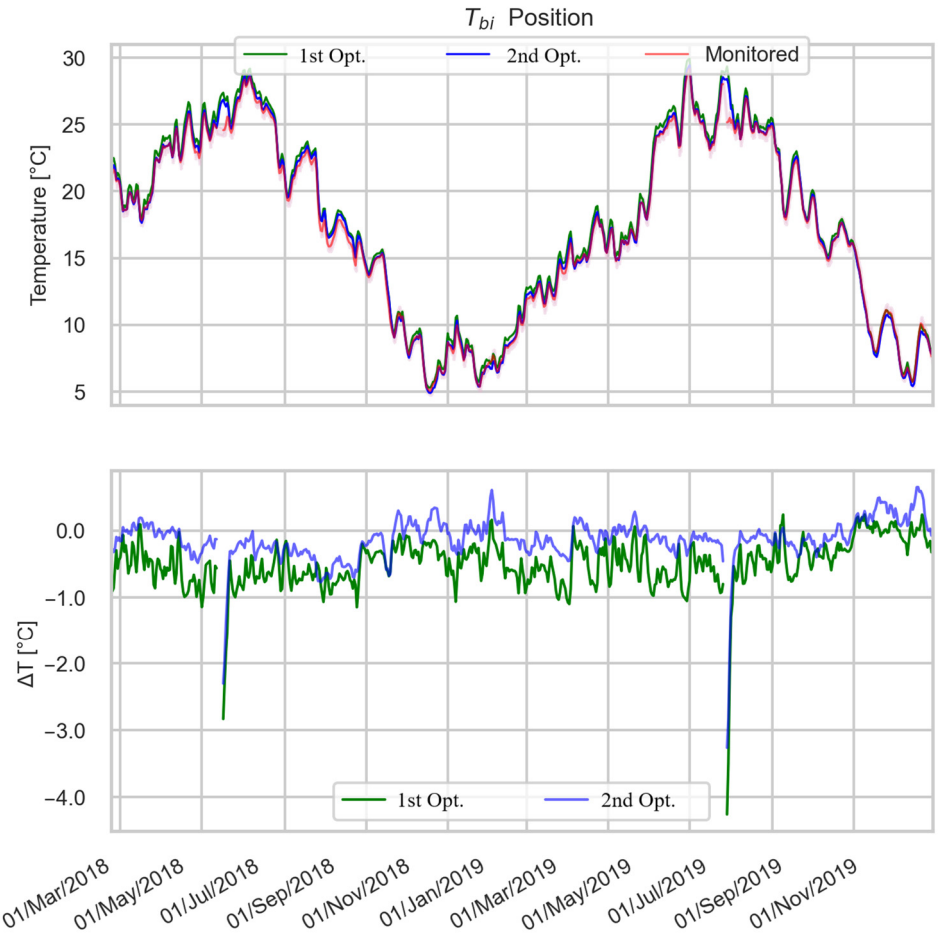

Figure 9. Comparison of the curve of the monitored temperature values at position T_{bi} (in red including the shadow air of the measurement uncertainty) with the curve of the first optimized simulation (in green) and the second optimized simulation (blue).

Figure 10 shows the temperature values at the position closest to the inner surface (T_{bip}). Moreover, in this position, the temperatures of the first optimized simulation are in general higher than the monitored ones (excluding the last month). The trend of the two simulations is very similar in both cases, but the second optimization produces a translation of the curve, bringing it closer to that of the monitored data. With respect to the T_{bip} position, the greatest discrepancy between the monitored and simulated values occurs during the winter months.

The extremely good agreement that is obtained between monitoring and simulation data during the whole monitoring period (which covers very diverse climatic conditions) demonstrates that the use of moisture independent thermal properties is a satisfying approximation for this specific case study. This can be related to the fact that the maximum relative humidity recorded by the sensors (not presented in this study) is 90%, whereas most materials accumulate significant amounts of moisture for values greater than 95%.

Considering the effects of humidity could still improve the calibration of the model and in another context (different climates, higher variation in moisture content during the year) it could be expected to play a more significant role.

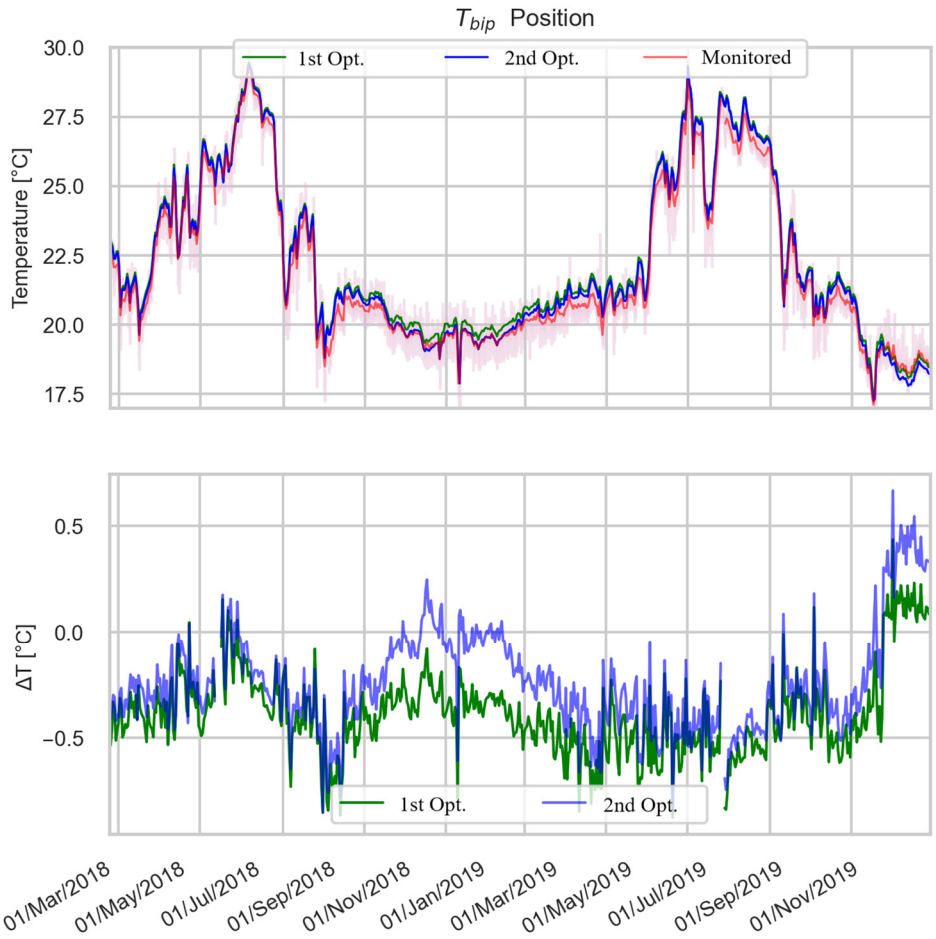

Figure 10. Comparison of the curve of the monitored temperature values at position T_{bip} (in red including the shadow air of the measurement uncertainty) with the curve of the first optimized simulation (in green) and the second optimized simulation (blue).

Lastly, the final values obtained for the input parameters at the end of the second step of the optimization process are analyzed. Figure 11 shows the values assumed by the material properties (thermal conductivity of insulation, new plaster, old plaster, and stone masonry and volumetric heat capacity of old plaster and stone) during the optimization process, while Figure 12 shows the same analysis for the coupling coefficients with the boundary conditions (internal convective heat transfer coefficient, external convective heat transfer coefficient, and the solar absorption coefficient).

In the graphs (Figures 11 and 12), each point represents the value assumed by the parameter (indicated in the graph title) for each simulation run through the optimization algorithm. The vertical red lines are the initial value of χ_{avg} corresponding to the first optimized simulation. The red triangle denotes the initial value of the varied parameter used in the first optimized simulation. The red circle corresponds to the best solution obtained with the second optimization process. The y-axis extends over the whole variation range used in the optimization process. The distribution of the cloud of points gives an indication of the degree of uncertainty which is associated with the final value obtained for the input parameters in the second optimization process. The faster the point swarm moves away from the second optimized value, the lower the degree of uncertainty.

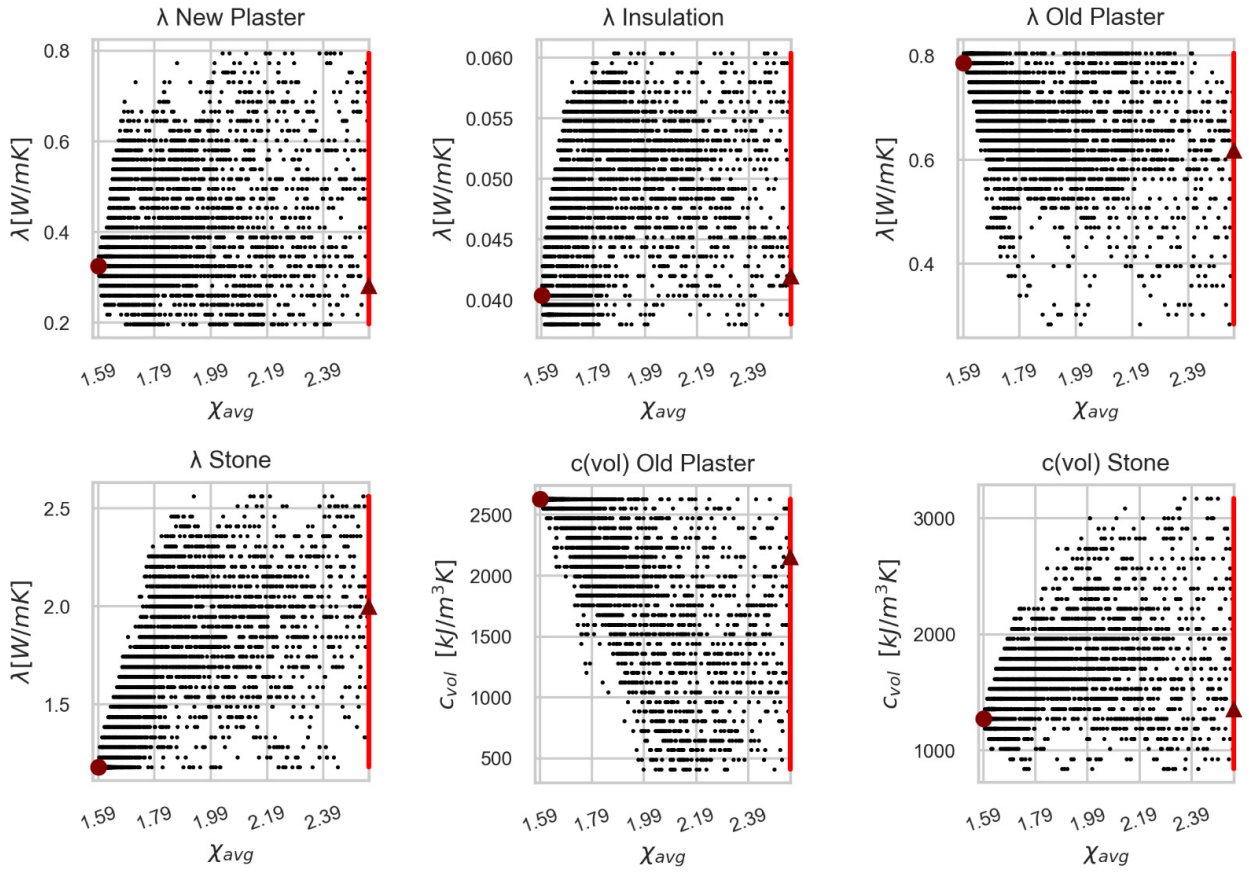

Figure 11. Overview of the second optimization results conducted on new plaster, old plaster, and stone masonry, in terms of thermal conductivity (λ) and volumetric heat capacity c_{vol}.

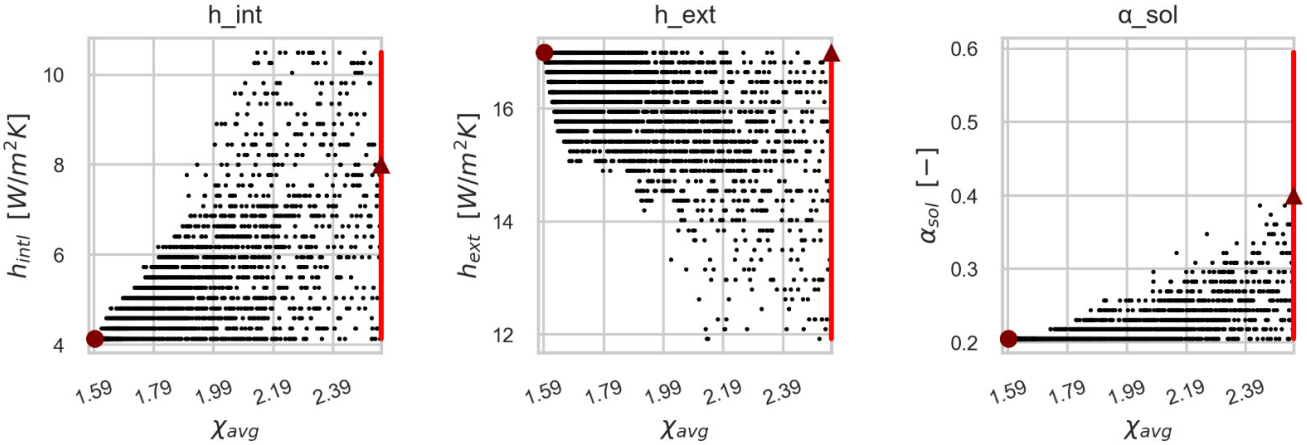

Figure 12. Overview of the second optimization results conducted on internal, external heat coefficient and the surface absorption coefficient.

In all graphs (excluding the one for α_{sol}) of Figures 11 and 12, it is possible to find optimization "attempts" within the whole variation range of the input parameters that have improved the first optimized simulation (which displays already a very good agreement with the monitored data). This suggests that the final values obtained in the second optimization process are not necessarily robust. Due to a large number of input parameters and the complexity of the problem the obtained input parameters may represent a set of values that maximize the agreement with the monitored data but do not necessarily represent the real physical values. It might be that the error made in the selection of a single

parameter may be balanced by the choice of the value of other parameters. When calibration is applied from monitored data, it is plausible to identify a set of input parameters that correspond only to one of the possible solutions. Compensation of input values can play a key role and make it difficult (if not impossible) to determine with certainty values that correspond to reality.

The difficulty in a robust determination of the value of the input parameters could be also related to the limited number of available monitored positions and to the fact that the boundary conditions (interior and exterior climate) are considered exact in this study. In fact, it is important to note that although the measured boundary conditions are undoubtedly extremely accurate, they are not error-free:

- The temperature of the indoor sensor is measured toward the interior of the room, a few meters away from the analyzed perimeter wall. As a result, the air temperature measured by the sensor may be higher than the air temperature close to the wall. A higher temperature would then cause the internal convective heat transfer coefficient to be overestimated in order to rebalance the model.
- The measured outside temperature may also be overestimated when solar radiation is present. In fact, although a radiation shield has been applied, it is known that it is very difficult to obtain a perfect screening. Therefore, with higher external air temperature, the model will underestimate the solar radiation and thus reduce the value of the radiation absorption coefficient.

The tendency of the swarm of values pointing to the optimal value is not the same for each parameter. Some graphs show that there are several "attempts" very close to the χ_{avg} optimized. A range of parameter variations can be identified graphically. Conceptually, this can be seen by comparing $\lambda_{insulation}$ and $c_{vol,stone}$.

4. Conclusions

The analysis performed in this paper supports the validation of the thermal simulation models used in dynamic simulation tools, by comparing their results with long-term monitoring data, and identifying the input parameters that affect the simulation results the most.

The analysis is applied to a renovated historical building located in Northern Italy (Settequerce-Bolzano/Bozen). For nearly two years, the temperature was monitored inside, outside, and in the stratigraphy of a wall insulated from the inside.

Using differential sensitivity analysis (DSA), this study quantifies the influence of input parameters of the thermal model. The results reveal that some parameters have a negligible impact on the output of the thermal simulation: these are the thermal properties of the glue layer, as well as the specific heat capacity and the density of the insulation and of the new plaster. Conversely, the most influential input parameters are the value of the coupling coefficients with the boundary conditions, as well as the thermal conductivity of all materials (except the one of the glue layer, as mentioned above).

The model validation is instead performed with a two-step calibration process. The first optimization step consists of an optimized selection of the materials in the Delphin database. The second optimization step implemented a more elaborated calibration process involving the variation of the single material thermal properties, as well as the internal and external coupling coefficients with the boundary conditions. A hybrid optimization algorithm composed of PSO (particle swarm optimization) and GSP (Hooke-Jeeves generalized pattern search) is used. The first optimization step resulted in a very good agreement between the simulated and monitored data. The second optimization step further improved the calibration leading to an excellent agreement.

Given this outcome, it can be concluded that the thermal model used in the dynamic simulation tool is reliable in describing and reproducing experimental data. In particular, the temperature output in the layer under the insulation (T_{bi}) showed excellent agreement with the monitored data. This represents a very positive outcome since an adequate

determination of the temperature behind the insulation is beneficial for the assessment of interstitial condensation.

The analysis of the optimization process performed in the second step showed that the final value obtained for the input parameters was not necessarily robust. In fact, the outcome of the optimization process revealed that there was a great deal of uncertainty in determining material parameters. The parameter values reported in the datasheets did not match those found through optimization. This means that even with extensive optimization using an algorithm, starting with monitoring data is insufficient to identify material parameter values. Indeed, very good curves can be obtained by changing the values of some parameters over very broad ranges. Based on this consideration and considering that the first optimization approach provided good agreement and is much faster, the authors conclude that the effort in implementing the second optimization step may not be justified.

Future scenarios could include additional parameters in the model calibration that were not considered in this study, such as the thickness of the materials. Furthermore, it is important to extend this thermal analysis to the hygric part considering the combined transport of heat and moisture in building components.

Author Contributions: The authors confirm the contributions to the paper as follows: Conceptualization, S.P., A.T., P.M.C. and M.L.; methodology, S.P., M.L. and A.T.; software, S.P. and M.L.; validation, S.P. and C.B.; formal analysis, S.P., C.B. and P.M.C.; investigation, S.P., M.L. and C.B.; resources, S.P., M.L. and A.T.; data curation, S.P., C.B. and M.L.; writing—original draft preparation, S.P. and C.B.; writing—review and editing, M.L., C.B., A.T. and P.M.C.; visualization, S.P., C.B. and P.M.C.; supervision, S.P., P.M.C. and A.T.; project administration, S.P., M.L. and C.B.; funding acquisition, A.T. and M.L. All authors have read and agreed to the published version of the manuscript.

Funding: This research received no external funding.

Institutional Review Board Statement: Not applicable.

Informed Consent Statement: Not applicable.

Data Availability Statement: Not applicable.

Acknowledgments: The authors would like to acknowledge the financial support for this research received through the HyLAB project, project funded by Provincia Autonoma di Bolzano–Alto Adige.

Conflicts of Interest: The authors declare no conflict of interest. The funders had no role in the design of the study; in the collection, analyses, or interpretation of data; in the writing of the manuscript; or in the decision to publish the results.

Nomenclature

Symbol	Title	Unit of Measure
h_{ext}	External convective heat transfer coefficient	W/m^2K
h_{int}	Internal convective heat transfer coefficient	W/m^2K
C_p	Heat capacity	J/kgK
T_{bep}	Position of sensors in the stratigraphy (behind the external plaster)	-
T_{bi}	Position of sensors in the stratigraphy (behind the insulation)	-
T_{bip}	Position of sensors in the stratigraphy (behind the internal plaster)	-
$T_{i,mon}$	Temperature recorded by the sensors	°C
$T_{i,sim}$	Hourly outcome in terms of temperature from the simulation	°C
c_{vol}	Volumetric heat capacity	kJ/m^3K

$e_{T_{i,mon}}$	Measurement uncertainty calculated as the maximum value between the instrument accuracy (± 0.3 °C) and the standard deviation (σ) between sensors placed in the same layer	°C
α_{sol}	Absorption coefficient for short waves radiation	-
χ_{RMSE}	Statistical index (equation 1)	-
$\chi_{T,bep}$	Statistical index related to the position T_{bep}	-
$\chi_{T,bi}$	Statistical index related to the position T_{bi}	-
$\chi_{T,bip}$	Statistical index related to the position T_{bip}	-
χ_{avg}	Average of the three calculated indices ($\chi_{T,bep}$, $\chi_{T,bi}$, $\chi_{T,bip}$)	-
DSA	Differential sensitivity analysis	-
SA	Sensitivity analysis	-
λ	Thermal conductivity	W/mK
ρ	Density	kg/m^3

References

1. Ceglia, F.; Marrasso, E.; Roselli, C.; Sasso, M. Time-Evolution and Forecasting of Environmental and Energy Performance of Electricity Production System at National and at Bidding Zone Level. *Energy Convers. Manag.* **2022**, *265*, 115772. [CrossRef]
2. Ceglia, F.; Marrasso, E.; Pallotta, G.; Roselli, C.; Sasso, M. The State of the Art of Smart Energy Communities: A Systematic Review of Strengths and Limits. *Energies* **2022**, *15*, 3462. [CrossRef]
3. D'Agostino, D.; Parker, D. Data on Cost-Optimal Nearly Zero Energy Buildings (NZEBs) across Europe. *Data Br.* **2018**, *17*, 1168–1174. [CrossRef] [PubMed]
4. Baglivo, C. Dynamic Evaluation of the Effects of Climate Change on the Energy Renovation of a School in a Mediterranean Climate. *Sustainability* **2021**, *13*, 6375. [CrossRef]
5. Bishara, N.; Pernigotto, G.; Prada, A.; Baratieri, M.; Gasparella, A. Experimental Determination of the Building Envelope's Dynamic Thermal Characteristics in Consideration of Hygrothermal Modelling—Assessment of Methods and Sources of Uncertainty. *Energy Build.* **2021**, *236*, 110798. [CrossRef]
6. Di Giuseppe, E.; D'Orazio, M.; Du, G.; Favi, C.; Lasvaux, S.; Maracchini, G.; Padey, P. A stochastic approach to LCA of internal insulation solutions for historic buildings. *Sustainability* **2020**, *12*, 1535. [CrossRef]
7. Pavlík, Z.; Maděra, J. Inverse Modeling of Thermal and Hygric Properties of Building Materials Based on a Semi-Scale Experiment. *Tpl. Fpv. Ukf. Sk* **2014**, 59–64. Available online: http://www.tpl.fpv.ukf.sk/engl_vers/thermophys/proceedings/pavlik_z.pdf (accessed on 15 August 2022).
8. Fiala, L.; Jerman, M.; Černý, R. Determination of material parameters of thermal insulation boards for the application on interior side of historical walls. *IOP Conf. Ser. Mater. Sci. Eng.* **2018**, *364*, 1. [CrossRef]
9. Coelho, G.B.A.; Henriques, F.M.A. Performance of Passive Retrofit Measures for Historic Buildings That House Artefacts Viable for Future Conditions. *Sustain. Cities Soc.* **2021**, *71*, 102982. [CrossRef]
10. Freudenberg, P.; Ruisinger, U.; Stöcker, E. Calibration of Hygrothermal Simulations by the Help of a Generic Optimization Tool. In *Energy Procedia*; Elsevier Ltd.: Amsterdam, The Netherlands, 2017; Volume 132, pp. 405–410. [CrossRef]
11. Congedo, P.M.; Baglivo, C.; D'Agostino, D.; Quarta, G.; Di Gloria, P. Rising Damp in Building Stones: Numerical and Experimental Comparison in Lecce Stone and Carparo under Controlled Microclimatic Conditions. *Constr. Build. Mater.* **2021**, *296*, 123713. [CrossRef]
12. Posani, M.; Veiga, M.D.R.; Peixoto de Freitas, V.; Kompatscher, K.; Schellen, H. Dynamic Hygrothermal Models for Monumental, Historic Buildings with HVAC Systems: Complexity Shown through a Case Study. *E3S Web Conf.* **2020**, *172*, 15007. [CrossRef]
13. Gutland, M.; Bucking, S.; Santana Quintero, M. Hygrothermal Modelling of Historic Rubble Masonry Walls: Accounting for Geometric and Compositional Variability. *J. Build. Eng.* **2022**, *48*, 103929. [CrossRef]
14. Ibrahim, M.; Sayegh, H.; Bianco, L.; Wurtz, E. Hygrothermal Performance of Novel Internal and External Super-Insulating Systems: In-Situ Experimental Study and 1D/2D Numerical Modeling. *Appl. Therm. Eng.* **2019**, *150*, 1306–1327. [CrossRef]
15. Ferreira, C.; Peixoto De Freitas, V.; Ramos, N.M.M. Quantifying the Influence of Hygroscopic Materials in the Fluctuation of Relative Humidity in Museums Housed in Old Buildings. *Stud. Conserv.* **2020**, *65*, 127–141. [CrossRef]
16. Chbani Idrissi, Y.; Belarbi, R.; Allam, R.; Feddaoui, M.; Bennai, F.; Agliz, D. Experimental and Numerical Validation of Hygrothermal Transfer in Brick Wall. *Heat Transf.* **2021**, *50*, 6300–6327. [CrossRef]
17. Costa-Carrapiço, I.; Croxford, B.; Raslan, R.; Neila González, J. Hygrothermal Calibration and Validation of Vernacular Dwellings: A Genetic Algorithm-Based Optimisation Methodology. *J. Build. Eng.* **2022**, *55*, 104717. [CrossRef]
18. Zhan, Q.; Xiao, Y.; Musso, F.; Zhang, L. Assessing the Hygrothermal Performance of Typical Lightweight Steel-Framed Wall Assemblies in Hot-Humid Climate Regions by Monitoring and Numerical Analysis. *Build. Environ.* **2021**, *188*, 107512. [CrossRef]
19. Andreotti, M.; Calzolari, M.; Davoli, P.; Dias Pereira, L. Hygrothermal Performance of an Internally Insulated Masonry Wall: Experimentations without a Vapour Barrier in a Historic Italian Palazzo. *Energy Build.* **2022**, *260*, 111896. [CrossRef]

20. Frasca, F.; Verticchio, E.; Cornaro, C.; Siani, A.M. Performance Assessment of Hygrothermal Modelling for Diagnostics and Conservation in an Italian Historical Church. *Build. Environ.* **2021**, *193*, 107672. [CrossRef]
21. Dong, W.; Chen, Y.; Bao, Y.; Fang, A. A Validation of Dynamic Hygrothermal Model with Coupled Heat and Moisture Transfer in Porous Building Materials and Envelopes. *J. Build. Eng.* **2020**, *32*, 101484. [CrossRef]
22. Coelho, G.B.A.; Silva, H.E.; Henriques, F.M.A. Calibrated Hygrothermal Simulation Models for Historical Buildings. *Build. Environ.* **2018**, *142*, 439–450. [CrossRef]
23. Sadłowska-Sałęga, A.; Radoń, J. Feasibility and limitation of calculative determination of hygrothermal conditions in historical buildings: Case study of st. Martin church in Wiśniowa. *Build. Environ.* **2020**, *186*, 1261–1269. [CrossRef]
24. Ueno, K.; Straube, J.; Van Straaten, R. Field monitoring and simulation of a historic mass masonry building retrofitted with interior insulation. In Proceedings of the 12th International Conference on Thermal Performance of the Exterior Envelopes of Whole Buildings, Clearwater, FL, USA, 1–5 December 2013.
25. Panico, S.; Larcher, M.; Troi, A.; Codreanu, I.; Baglivo, C.; Congedo, P.M.; Suzuki, S.; Tanahashi, T.; Panico, S.; Larcher, M.; et al. Hygrothermal Analysis of a Wall Isolated from the inside: The Potential of Dynamic Hygrothermal Simulation. In Proceedings of the IOP Conference Series: Earth and Environmental Science, Raipur, India, 1 October 2021; Volume 863, p. 012053.
26. Grint, N.; Marincioni, V.; Elwell, C.A. Sensitivity and Uncertainty Analyses on a DELPHIN Model: The Impact of Material Properties on Moisture in a Solid Brick Wall. *E3S Web Conf.* **2020**, *172*, 04006. [CrossRef]
27. Roberti, F.; Oberegger, U.F.; Gasparella, A. Calibrating Historic Building Energy Models to Hourly Indoor Air and Surface Temperatures: Methodology and Case Study. *Energy Build.* **2015**, *108*, 236–243. [CrossRef]
28. Nielsen, A.; Møller, E.B.; Rasmussen, T.V.; de Place Hansen, E.J. Use of Sensitivity Analysis to Evaluate Hygrothermal Conditions in Solid Brick Walls with Interior Insulation. In Proceedings of the 5th International Building Physics Conference (IBPC): The Role of Building Physics in Resolving Carbon Reduction Challenge and Promoting Human Health in Buildings, Kyoto, Japan, 28 May 2012.
29. Marincioni, V.; Marra, G.; Altamirano-Medina, H. Development of Predictive Models for the Probabilistic Moisture Risk Assessment of Internal Wall Insulation. *Build. Environ.* **2018**, *137*, 257–267. [CrossRef]
30. Pernetti, R. *On the Influence of Several Parameters in Energy Model Calibration: The Case of a Historical Building*; IBPSA: Torino, Italy, 2013; pp. 263–272.
31. Zheng, O.; Eisenhower, B. Leveraging the Analysis of Parametric Uncertainty for Building Energy Model Calibration. *Build. Simul.* **2013**, *6*, 365–377. [CrossRef]
32. Kramer, R.; van Schijndel, J.; Schellen, H. Inverse Modeling of Simplified Hygrothermal Building Models to Predict and Characterize Indoor Climates. *Build. Environ.* **2013**, *68*, 87–99. [CrossRef]
33. Jensen, N.F.; Bjarløv, S.P.; Rode, C.; Møller, E.B. Hygrothermal Assessment of Four Insulation Systems for Interior Retrofitting of Solid Masonry Walls through Calibrated Numerical Simulations. *Build. Environ.* **2020**, *180*, 107031. [CrossRef]
34. Grint, N.; Elwell, C.A. Moisture in walls before and after internal wall insulation: A long-term in-situ dataset. In *E3S Web of Conferences*; EDP Sciences: Paris, France, 2020; Volume 172. [CrossRef]
35. Delphin 6.1 Technische Universität Dresden-Institut fur Bauklimatik. *Delphin 6.1 Material Database*; Institut für Bauklimatik Technische Universität: Dresden, Germany, 2013.
36. Congedo, P.M.; Baglivo, C.; Seyhan, A.K.; Marchetti, R. Worldwide Dynamic Predictive Analysis of Building Performance under Long-Term Climate Change Conditions. *J. Build. Eng.* **2021**, *42*, 103057. [CrossRef]
37. WTA. *Simulation of Heat and Moisture Transfer*; WTA: St. Petersburg, FL, USA, 2014.
38. *DIN V 18599-1:2018-09*; Energy Efficiency of Buildings—Calculation of the Net, Final and Primary Energy Demand for Heating, Cooling, Ventilation, Domestic Hot Water and Lighting—Part 1: General Balancing Procedures, Terms, and Definitions, Zoning and Evaluation of Energy Source. Deutsches Institut für Normung: Berlin, Germany, 2018.
39. Huerto-Cardenas, H.E.; Leonforte, F.; Aste, N.; Del Pero, C.; Evola, G.; Costanzo, V.; Lucchi, E. Validation of Dynamic Hygrothermal Simulation Models for Historical Buildings: State of the Art, Research Challenges and Recommendations. *Build. Environ.* **2020**, *180*, 107081. [CrossRef]
40. Saltelli, A.; Tarantola, S.; Campolongo, F.; Ratto, M. *Sensitivity Analysis in Practice: A Guide to Assessing Scientific Models*; Wiley: Chichester, UK, 2004.
41. Choi, H.-J.; Kang, J.-S.; Huh, J.-H. A Study on Variation of Thermal Characteristics of Insulation Materials for Buildings According to Actual Long-Term Annual Aging Variation. *Int. J. Thermophys.* **2017**, *39*, 2. [CrossRef]
42. *ISO 10456:2007*; Building Materials and Products. Hygrothermal Proprieties. Procedure for Determining the Design Values. ISO: Milan, Italy, 2015.
43. Desogus, G. The effects of mortar on the dynamic thermal performances of stone masonries. *Riv. TEMA* **2021**, *7*, 77–85. [CrossRef]
44. Pascucci, M.; Lucchi, E. *2D-Hygrothermal Simulation of Historical Solid Walls*; Periodica Polytechnica Budapest University of Technology and Economics: Budapest, Hungary, 2016; pp. 155–161.
45. Bottino-Leone, D.; Larcher, M.; Troi, A.; Grunewald, J. Hygrothermal Characterization of a Fictitious Homogenized Porous Material to Describe Multiphase Heat and Moisture Transport in Massive Historic Walls. *Constr. Build. Mater.* **2021**, *266*, 121497. [CrossRef]
46. *UNI EN ISO 10456*; Materiali e Prodotti Per edilizia: Proprietà Igrometriche: Valori Tabulati Di Progetto e Procedimenti Per La Determinazione Dei Valori Termici Dichiarati e Di Progetto. ISA: Milan, Italy, 2008.

47. *UNI EN ISO 13788*; Prestazione Igrotermica Dei Componenti e Degli Elementi Per Edilizia–Temperatura Superficiale Interna Per Evitare l'umidità Superficiale Critica e Condensazione Interstiziale–metodo di calcolo. ISA: Milan, Italy, 2013.
48. WUFI. *Material Database*; WUFI: Holzkirchen, Germany, 2017.
49. Wetter, M. GenOpt®-A Generic Optimization Program GenOpt Ö-A Generic Optimization Program. 2001. Available online: http://simulationresearch.lbl.gov (accessed on 24 June 2021).